LA-UR-16-22749
Approved for public release; distribution is unlimited.

Title: A Complete Reporting of MCNP6 Validation Results for Electron Energy Deposition in Single-Layer Extended Media for Source Energies <= 1-MeV

Author(s): Dixon, David A.
Hughes, Henry Grady III

Intended for: Report

Issued: 2016-05-04 (rev.1)

A Complete Reporting of MCNP6 Validation Results for Electron Energy Deposition in Single-Layer Extended Media for Source Energies $\leq$ 1-MeV

David A. Dixon and H. Grady Hughes
Los Alamos National Labs
XCP-3, Monte Carlo Methods and Apllications Group

May 3, 2016

1 Introduction

In this paper, we expand on previous validation work by Dixon and Hughes [1]. That is, we present a more complete suite of validation results with respect to to the well-known Lockwood energy deposition experiment [2]. Lockwood *et al.* measured energy deposition in materials including beryllium, carbon, aluminum, iron, copper, molybdenum, tantalum, and uranium, for both single- and multi-layer 1-D geometries. Source configurations included mono-energetic, mono-directional electron beams with energies of 0.05-MeV, 0.1-MeV, 0.3-MeV, 0.5-MeV, and 1-MeV, in both normal and off-normal angles of incidence. These experiments are particularly valuable for validating electron transport codes, because they are closely represented by simulating pencil beams incident on 1-D semi-infinite slabs with and without material interfaces. Herein, we include total energy deposition and energy deposition profiles for the single-layer experiments reported by Lockwood *et al.* (a more complete multi-layer validation will follow in another report).

MCNP6 transports electrons primarily through an application of the condensed history (CH) algorithm [3]. By default, CH is applied to electrons with energies above 1-keV; however, recent improvements in the MCNP6 electron transport include the ability to use a single-event or analog algorithm [4]. However, the emphasis of this paper is the validation of the default algorithm, or condensed history. Therefore, we did not include the impact of adjusting parameters such as *ESTEP* or *EFAC*. While the impact of *ESTEP* or *EFAC* parameters are not presented herein, we did study them and found that agreement with the experimental benchmark was not greatly improved (in several cases refinement of *EFAC* worsened agreement).

In the following sections, the Lockwood energy deposition experiment is described and details from the experiment pertinent to generating the necessary MCNP6 input decks are noted. Characteristics of the simulation including the geometry and materials, physics parameters, source configuration, and so on are summarized. Validation results are presented

and followed by concluding remarks on the status of the energy deposition validation with recommendations for potential improvements to the MCNP6 CH algorithm.

2 The Lockwood Energy Deposition Data

The Lockwood energy deposition experiments [2] were motivated by the presence of ambiguities in traditional methods during the early 1970s. In particular, much of the published data reported some response profile other than energy deposition or the data was normalized to agree with other available results; many results were obtained in infinite rather than semi-infinite media to simplify experimental considerations; very little data existed for source energies less than 1.0-MeV in semi-infinite slabs; and spatial resolution in experiments for semi-infinite geometries were poor near the surface.

To improve upon previous experimental measurements, Lockwood *et al.* employed a thin-foil calorimetric technique that did not require any stopping power corrections and eliminated the need for a window (both required by gas-filled ionization chambers) because the device could be placed in vacuo. While the new approach devised by Lockwood *et al.* was a great improvement, the data is still subject to experimental uncertainties (ranging from 1% to 3% [2]).

Energy deposition profiles were determined by placing foils with increasing thickness between an accelerator beam and a calorimeter foil, where heating in the foil was converted to energy deposited. This is shown in the schematic for single-layer measurements in Fig. 1. The spatial location of energy deposited was reported as the thickness of the front foils plus one-half the thickness of the calorimeter foil. A cross-section of the calorimeter foil and the front foil would reveal that they are both eight-sided polygons. The largest dimension of the calorimeter foil is reported as 8.25-cm and the largest dimension of the front foil is 8.89-cm (detailed drawings with dimensions are given in [2]). Note the gaps between the front foil, calorimeter foil, and the infinite plate, which are reported as 0.1-cm. In some cases, thin aluminum foils were placed on either side of the calorimeter to reduce thermal coupling effects; however, those are neglected herein. The more detailed experimental apparatus is given in Lockwood *et al.* [2], but only the components used in the simulation are discussed below.

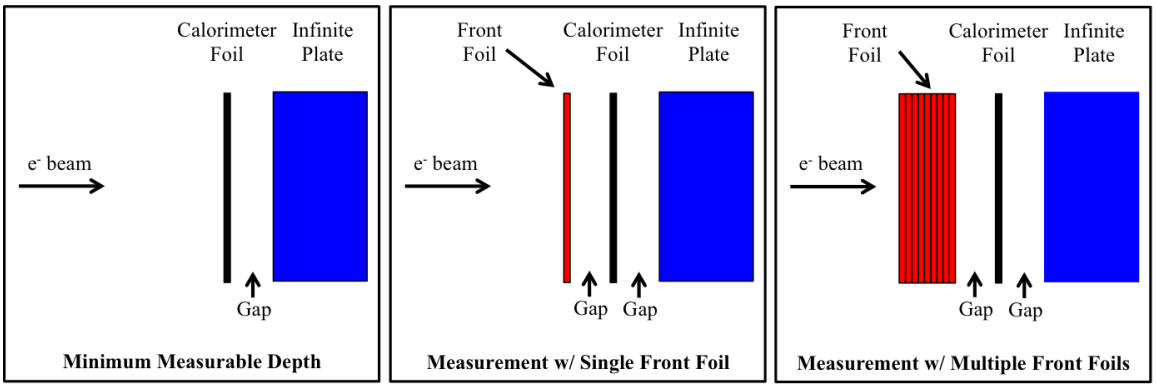

Figure 1: Simple schematic of thin calorimeter approach.

The electron source is a collimated accelerator beam with energy resolution reported as approximately 0.1% and uncertainty in the angle of incidence are reported as less than 0.5%. However, the beam width and angular spreading of the beam is not reported (a beam diameter of 0.02 mm is provided in an previous report [5], but not the final report [2]). That said, the version of ITS used to generate the theoretical energy deposition profiles in Lockwood *et al.* was the TIGER code, the 1-D version of ITS, leading one to believe that the experimental source configuration was intended to be a close representation of a pencil beam.

The experimental results are reported at points even though the calorimeter foils have a finite width. One could convert the experimental results into histograms by determining the calorimeter foil thickness and assuming that energy deposition across the thin calorimeter foil is constant. However, one will find many cases where the histograms overlap. The overlap is a result of the experimental setup. That is, the calorimeter foil is of constant thickness and the front foils are of varying thicknesses. In the event that the front foil is increased by a thickness that is less than the calorimeter foil thickness, the experimental values will overlap if one choses to interpret the experimental values as histograms with thicknesses given by the calorimeter foil as opposed to points.

In the following section, the various assumptions made to complete the validation are explained. Namely, we discuss geometric considerations and their impact on results.

3 SIMULATION CHARACTERISTICS

Given a brief description of the experiment, the simulations reported herein are now described. Specifically, the details necessary to reproduce the input files are described. This includes a discussion of the geometry, source specifications, tally requirements, and physics parameters.

Simulations were completed with a geometric model that was intended to be a reasonably close representation of the actual experiment. In each simulation, a front foil is placed between the beam and the calorimeter foil, which is followed by an infinite plate (with exception of the minimum measurable depth). In subsequent simulations, the front foil thickness is increased (see Fig. 1) such that it is consistent with the experimental results, or according the following formula:

$$(\Delta x)_i^{ff} = x_i^{exp} - \frac{(\Delta x)_j^{cal}}{2}, \tag{1}$$

where $(\Delta x)_i^{ff}$ is the ith front foil thickness, x_i^{exp} is the ith x-position of the experimental energy deposition profile reported by Lockwood *et al.*, and $(\Delta x)_j^{cal}$ is the calorimeter thickness for the jth material. The front foil thickness is determined for each simulation such that the dose can be compared point-wise with the experimental results. Therefore, each simulation corresponds to specific experimental data point, and multiple simulations are required for each energy deposition profile. For example, if the experimental energy deposition profile is reported at 15 different spatial points, then 15 simulations are required to reproduce these results.

The default physics parameters, or the physics cards for electrons and photons, were not modified for the results reported herein. These parameters are reported in the manual [6], but are included nonetheless. In the physics card one can control the various mechanisms by which electrons and photons interact, and the result of such interactions. A brief list

includes knock-on electrons, bremsstrahlung, Compton electrons, straggling logic, number of substeps per energy step, and so on. By default, MCNP6 transports all of the aforementioned secondary radiation. In addition, the default low energy threshold for condensed history transport was used. This coincides with the 1-keV default threshold for activating the single-event electron transport (1-keV is also the default threshold for photons).

The electron source was assumed to be a pencil beam located at the origin. Angles of incidence included normal, 30°off-normal, or 60°. Source energies were evaluated at 0.05-, 0.1-, 0.3, 0.5, and 1.0-MeV depending of the material of interest. Finally, in each simulation, 10^6 histories were followed resulting in statistical uncertainties well-below the experimental uncertainty (with exception of a few simulations where the last few cells were not sufficiently sampled, but the energy deposited in these cells is negligible.)

4 Results

In this section, we present validation results for total energy deposition and energy deposition profiles in single-layer slabs composed of elemental materials. In tables 1-3, total energy deposition is presented[1]. There are three sources of total energy deposition presented. The first, noted as "Lockwood Report," corresponds to the total energy deposition values reported in Lockwood *et al.* [2]. Lockwood *et al.* obtained these values by fitting the experimental results, evaluating the fit at many points, and applying a simple rectangular integration technique to the evaluation of the fit. The other two total energy deposition values presented are noted as "Experiment" and "MCNP6." These values are obtained by applying a polynomial fitting technique using *polyfit* and *poly1d* from *NumPy* - see Figs. 2 - 14 for examples of the fits. The total energy deposition results noted as "Experiment" and "MCNP6" are obtained by evaluating each fit at 1000 points on the interval of interest and applying a rectangular integration technique consistent with Lockwood *et al.*

In general, all three results tend to agree to within 5%. That said, if we assume results corresponding to "Experiment" are the benchmark, there are six cases with disagreement ranging from roughly 5-10% and one where the disagreement is roughly 16%. As it is difficult to identify a single source of disagreement in integral calculations such as energy deposition, we will simply note the cases with significant disagreement and revisit the validation given future modifications the MCNP6 electron-photon transport algorithm to determine if agreement was improved.

As noted, Figs. 2 - 14 (see appendices) contain plots of the energy deposition profiles (experimental and calculated). The experimental results are point-wise plots, while the calculated result is fitted to distinguish between the two. Energy deposition profiles were generated only for source energies greater than or equal to 0.3-MeV because at lower energies spatial resolution for the experimental results only include a few points (and in some cases only one point). In addition to the energy deposition profiles, the appendices contain relative difference plots for each result in this section. These relative difference plots are better suited for reporting the lower energy results, so they are included in these figures as well.

[1] In most Be cases, the total energy deposited is non-conservative which is likely a result of the integration technique.

Table 1: Total energy deposition from **normally** incident sources. Results include total energy deposited reported in Lockwood *et al.* [2], and total energy deposition obtained by fitting and integrating the experimental results from Lockwood *et al.* and MCNP6 simulations.

		Total Energy Deposition (MeV)		
Material	Particle Energy (MeV)	Lockwood Report	Experiment	MCNP6
Be	0.05	0.049	0.049	0.049
	0.10	0.109	0.116	0.098
	0.30	0.312	0.308	0.299
	0.50	0.520	0.515	0.501
	1.00	1.022	1.006	1.005
C	1.00	0.987	0.966	0.977
Al	0.05	0.049	0.049	0.046
	0.10	0.039	0.039	0.041
	0.30	0.285	0.286	0.281
	0.50	0.479	0.542	0.472
	1.00	0.970	0.953	0.956
Fe	0.30	0.242	0.239	0.250
	0.50	0.404	0.401	0.424
	1.00	0.804	0.800	0.869
Cu	0.30	0.242	0.234	0.240
	0.50	0.412	0.409	0.414
Mo	0.10	0.069	0.071	0.071
	0.30	0.208	0.208	0.225
	0.50	0.373	0.372	0.384
	1.00	0.779	0.781	0.798
Ta	0.30	0.184	0.201	0.181
	0.50	0.316	0.314	0.310
	1.00	0.648	0.635	0.662
U	0.30	0.165	0.163	0.165
	0.50	0.277	0.279	0.285
	1.00	0.584	0.585	0.560

Table 2: Total energy deposition from **30 degrees off-normal** sources. Results include total energy deposited reported in Lockwood *et al.* [2], and total energy deposition obtained by fitting and integrating the experimental results from Lockwood *et al.* and MCNP6 simulations.

		Total Energy Deposition (MeV)		
Material	Particle Energy (MeV)	Lockwood Report	Experiment	MCNP6
Ta	0.30	0.177	0.243	0.240

Table 3: Total energy deposition from **60 degrees off-normal** sources. Results include total energy deposited reported in Lockwood *et al.* [2], and total energy deposition obtained by fitting and integrating the experimental results from Lockwood *et al.* and MCNP6 simulations.

		Total Energy Deposition (MeV)		
Material	Particle Energy (MeV)	Lockwood Report	Experiment	MCNP6
Al	0.30	0.230	0.224	0.212
	0.50	0.391	0.381	0.382
	1.00	0.759	0.745	0.758
Mo	0.30	0.160	0.149	0.155
	0.50	0.272	0.263	0.277
	1.00	0.557	0.557	0.599
Ta	0.50	0.227	0.182	0.187
	1.00	0.472	0.428	0.446
U	1.00	0.413	0.384	0.408

5 Conclusions

In this work, energy deposition profiles generated using the MCNP6 electron-photon transport algorithms were compared to the Lockwood experiment. Generally, the MCNP6 electron-photon transport algorithms agree well with experiment when calculating total energy deposition (i.e. energy deposition in regions on the order of the mean range of an electron for a given source energy from 0.05- to 1.0-Mev). However, in many of the materials tested, the peak dose was overestimated and the tail of the energy deposition profile was underestimated. Energy deposition is an integral quantity, so it is difficult to identify a single-source of error. However, future validation work that isolates the individual components of the MCNP6 algorithm may lead to modifications of the various components. Given improvements to the various components, this validation will be revised to determine how the improvements impact energy deposition calculations.

In connection with this work, Dixon and Hughes studied the impact of various physics parameters on these validation results and found that they do not have a significant impact [1]. A general recommendation is to avoid changing defaults when using MCNP6 for energy deposition calculations in the presence of mono-energetic, mono-directional source electrons 1-MeV and below. This recommendation likely extends to more complex sources within the energy range of 0.05- to 1.0-MeV.

Results from this study and the previous study [1] led to the following recommendations specific to energy deposition calculations: do not override the default number of substeps via *ESTEP*, unless cells are smaller than one substep; do not override the default straggling model, DBCN(18)=2; and do not override the default energy grid, *EFAC*.

Additional work pertinent to this benchmark includes a study of the sensitivity of energy deposition to the underlying angular distributions, alternative boundary crossing approximations, and the use of the MCNP6 single-event methodology for electron transport.

References

[1] D. Dixon and H.G. Hughes. Validation of mcnp6 for electron energy deposition in extened media. *Trans. Am. Nucl. Soc.*, 2015.

[2] G. J. Lockwood, L. E. Ruggles, G. H. Miller, and J. A. Halbleib. Calorimetric measurement of electron energy deposition in extended media– theory vs experiment. Technical Report SAND79-0414, SNL, 1987.

[3] M.J. Berger. Monte Carlo calculation of the penetration and diffusion of fast charged particles. In *Methods in Computational Physics*, volume 1 of *Statistical Physics*, pages 135–215. Advances in Research and Applications, Academic Press, 1963.

[4] H. G. Hughes. Recent developments in low-energy electron/photon transport for mcnp6 - revision 4. Technical Report LA-UR-12-24213 rev 4, Los Alamos National Laboratory, 2013.

[5] G. J. Lockwood, G. H. Miller, and J. A. Halbleib. Electron energy deposition in multilayer geometries. *IEEE Trans. Nucl. Sci.*, NS-23(6):1862–1866, 1976.

[6] X-5 Monte Carlo Team. Mcnp - a general n-particle transport code, version 5 - volume i: Overview and theory. Technical Report LA-UR-03-1987, Los Alamos National Laboratory, 2003.

Appendices

A Energy Deposition Profiles

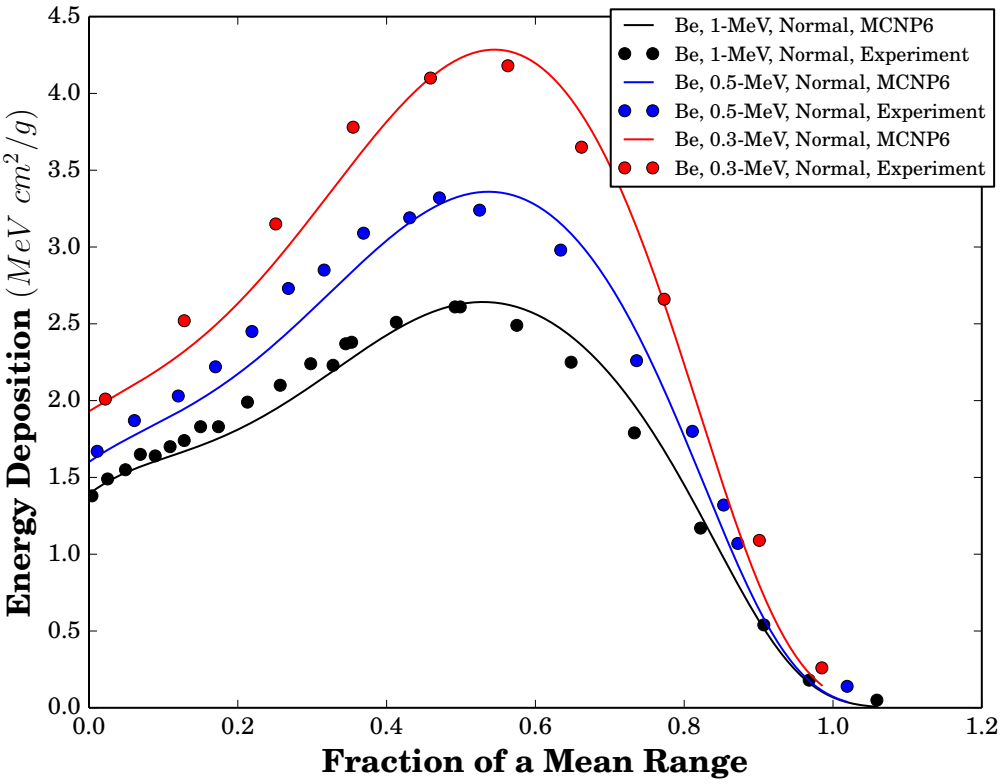

Figure 2: Energy deposition from 0.3- to 1-MeV electrons normally incident on a Be single-layer slab.

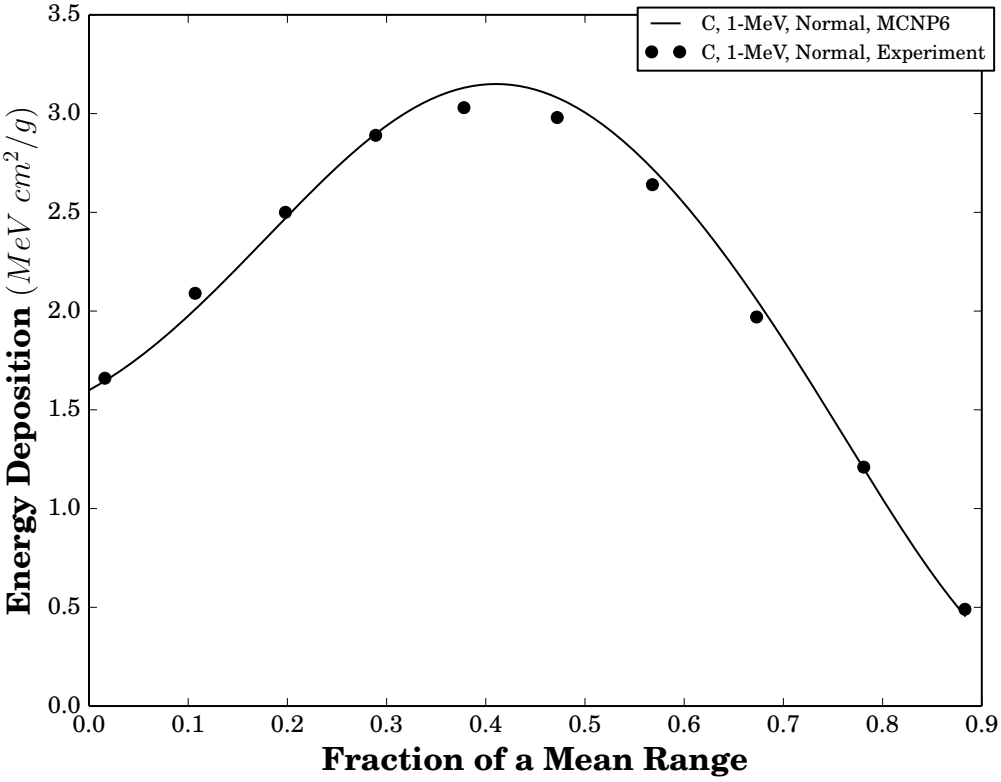

Figure 3: Energy deposition from 1-MeV electrons normally incident on a C single-layer slab.

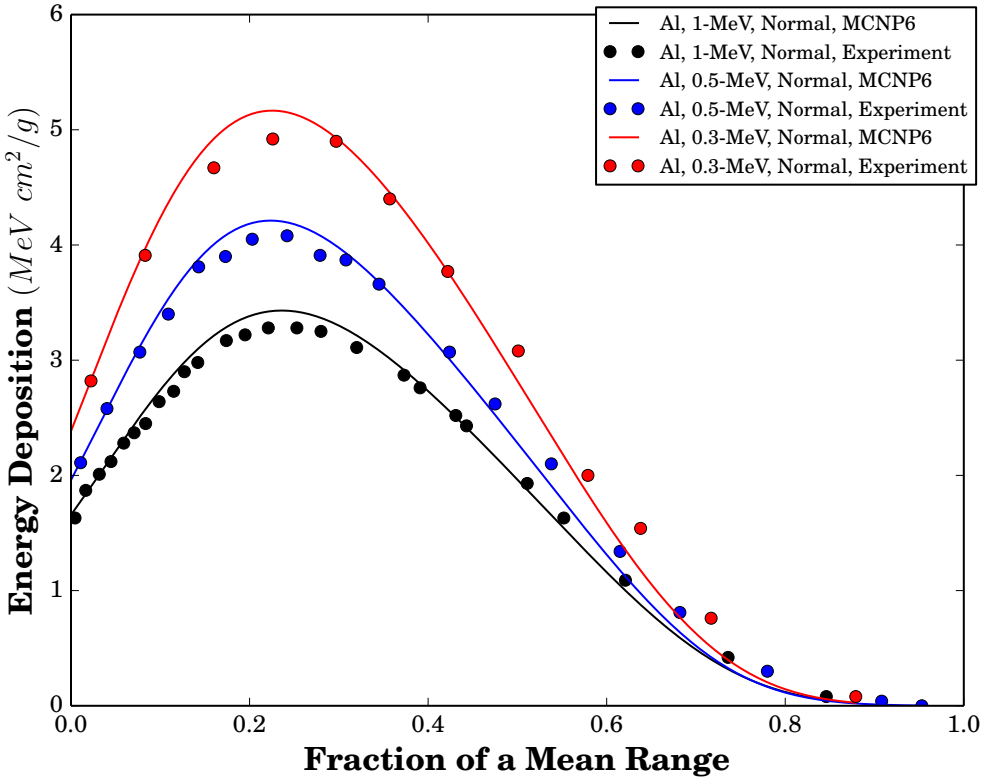

Figure 4: Energy deposition from 0.3- to 1-MeV electrons on a normally incident Al single-layer slab.

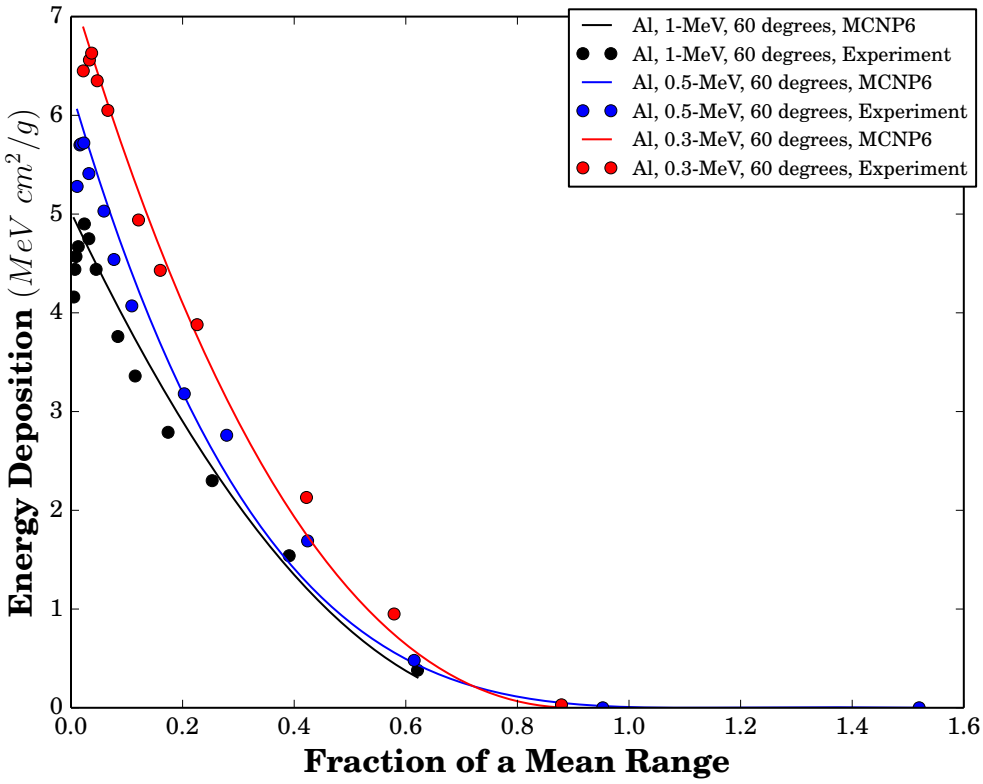

Figure 5: Energy deposition from 0.3- to 1-MeV electrons with 60 degrees off-normal incidence on a Al single-layer slab.

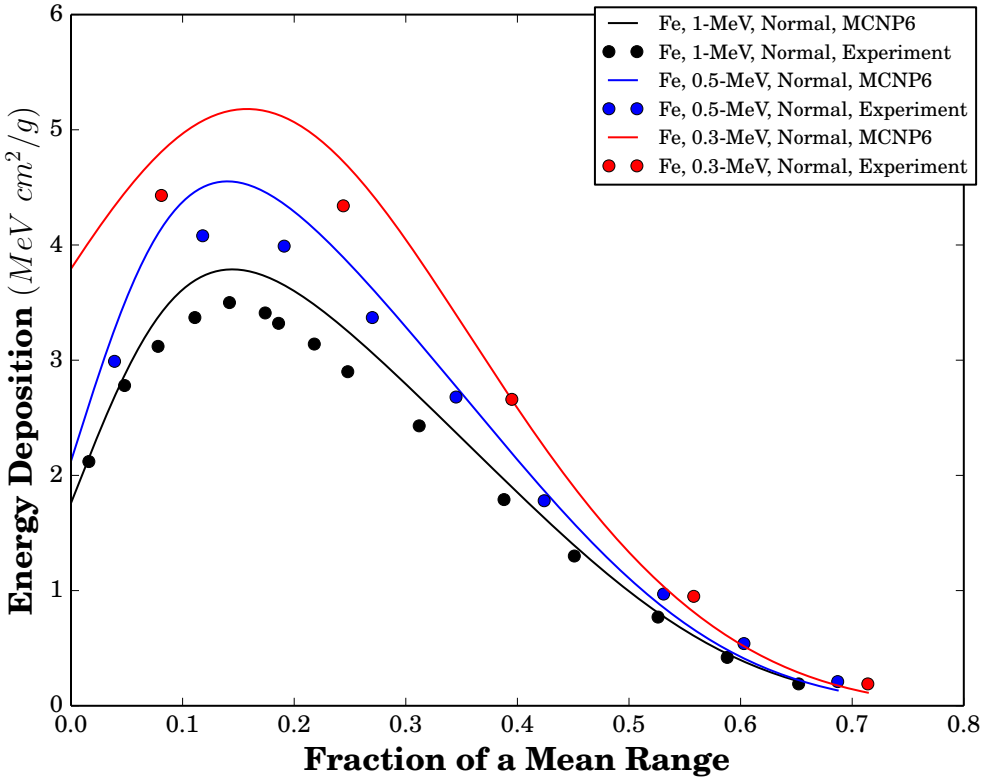

Figure 6: Energy deposition from 0.3- to 1-MeV electrons normally incident on a Fe single-layer slab.

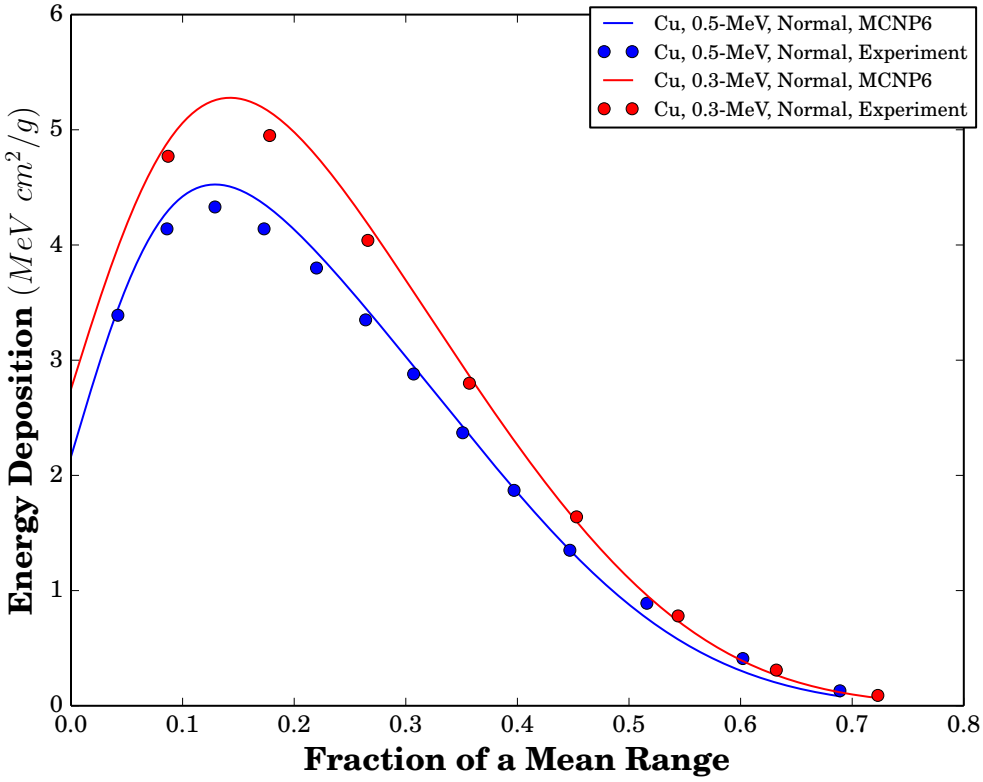

Figure 7: Energy deposition from 0.3- to 0.5-MeV electrons normally incident on a Cu single-layer slab.

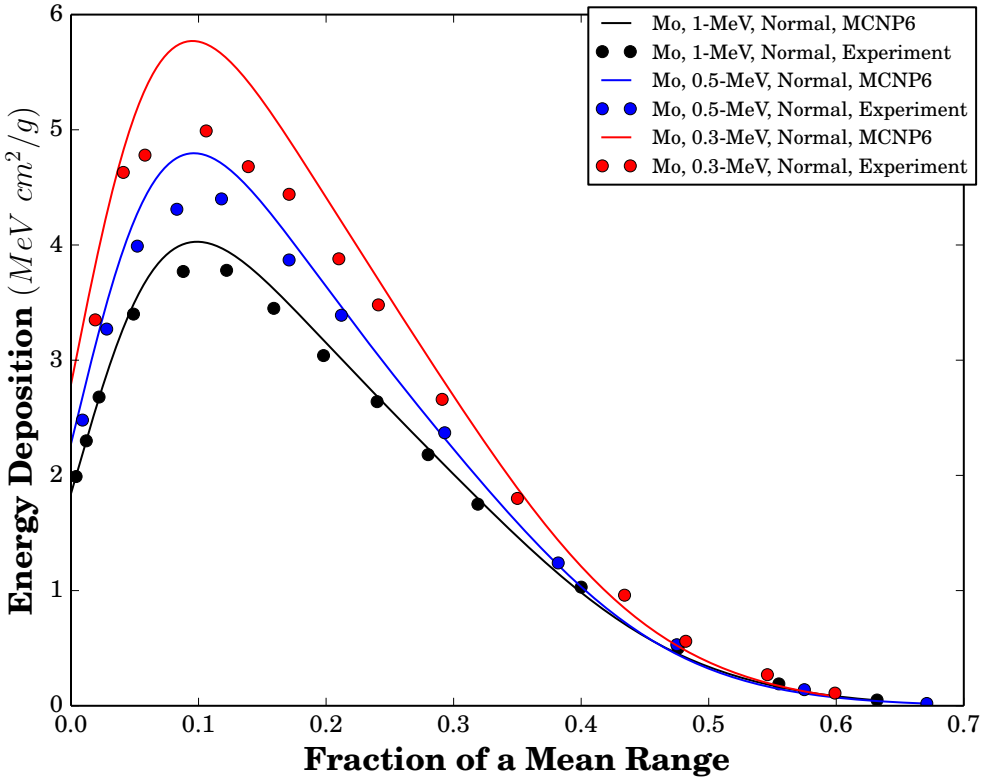

Figure 8: Energy deposition from 0.3- to 1-MeV electrons normally incident on a Mo single-layer slab.

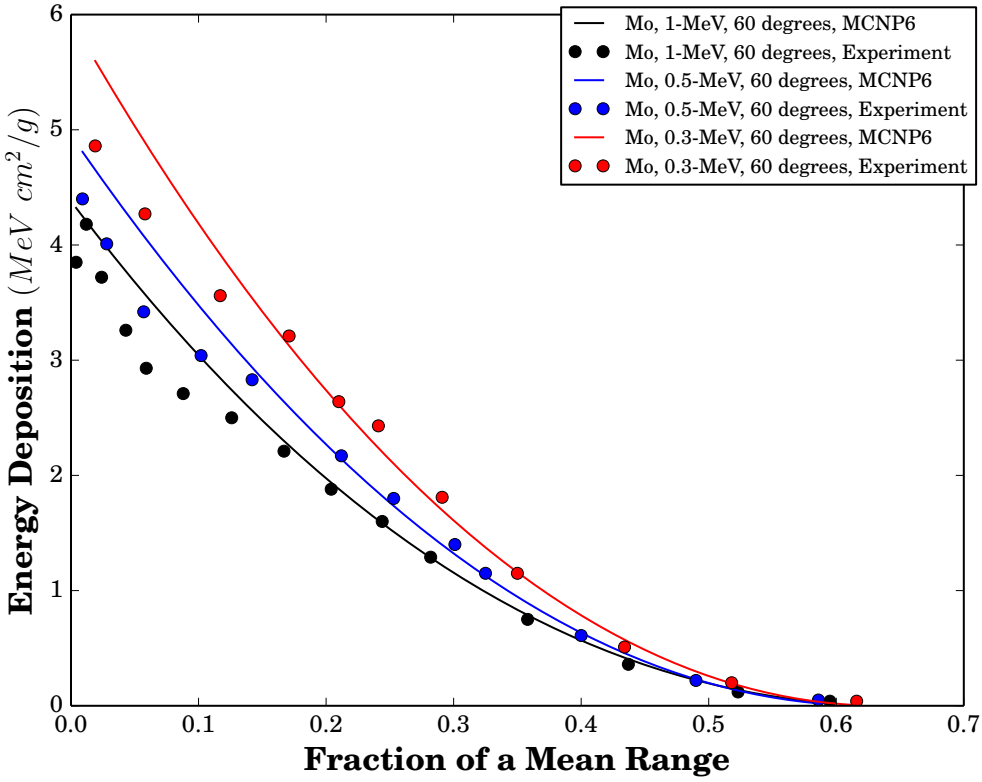

Figure 9: Energy deposition from 0.3- to 1-MeV electrons with 60 degrees off-normal incidence on a Mo single-layer slab.

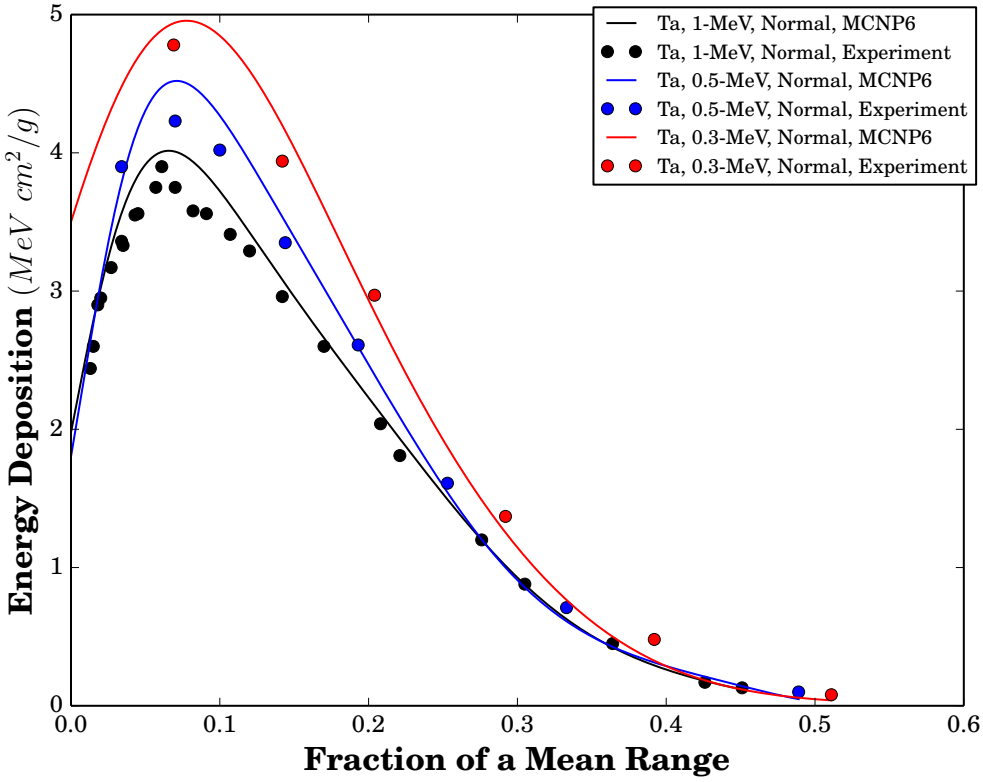

Figure 10: Energy deposition from 0.3- to 1-MeV electrons normally incident on a Ta single-layer slab.

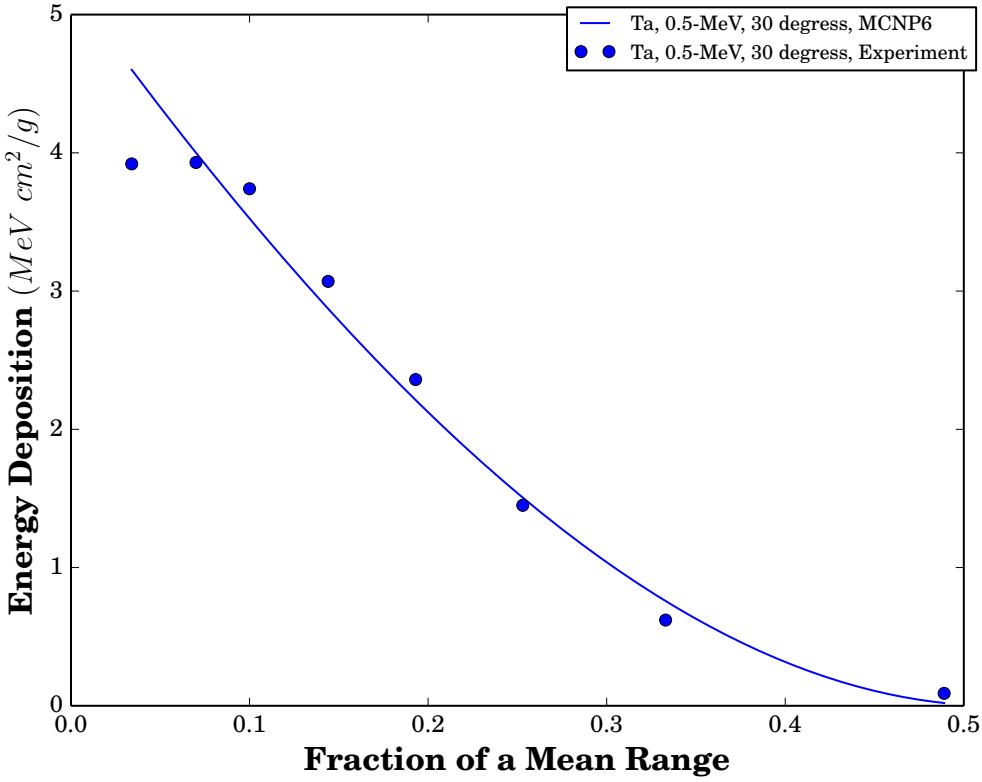

Figure 11: Energy deposition from 0.3- to 1-MeV electrons with 30 degrees off-normal incidence on a Ta single-layer slab.

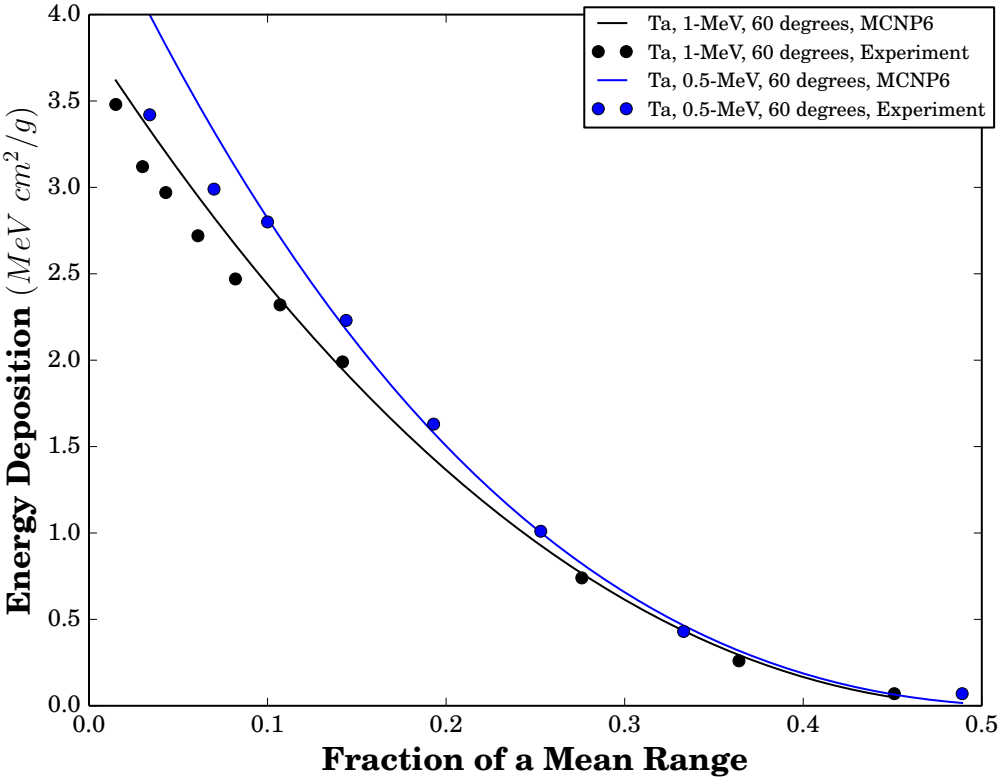

Figure 12: Energy deposition from 0.3- to 1-MeV electrons with 60 degrees off-normal incidence on a Ta single-layer slab.

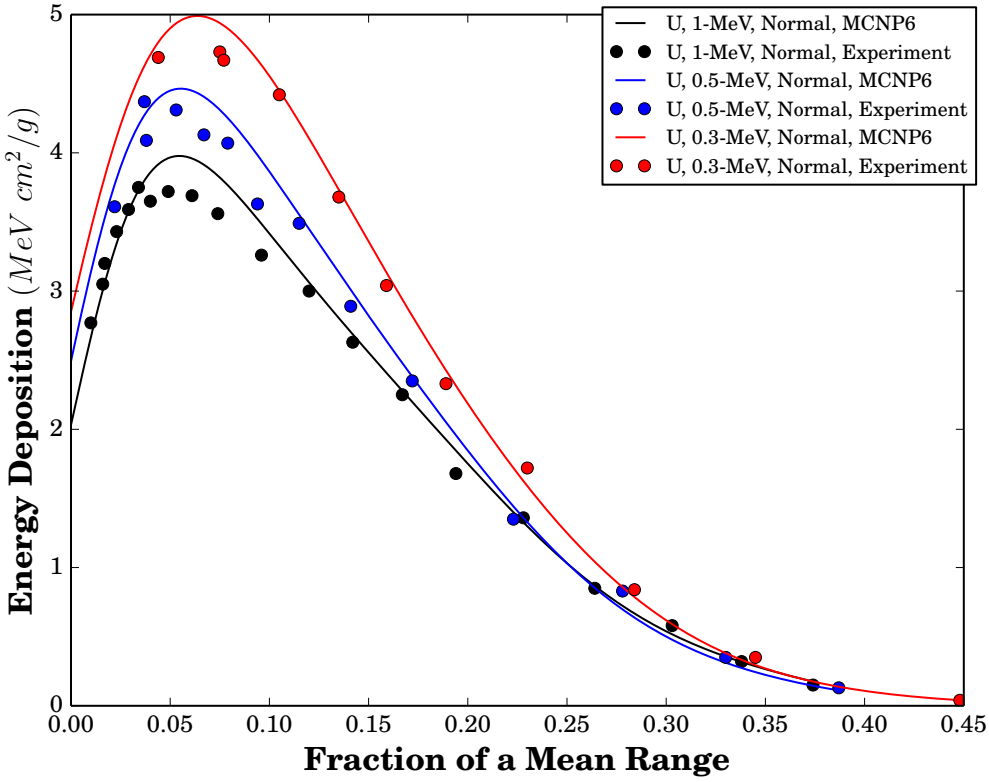

Figure 13: Energy deposition from 0.3- to 1-MeV electrons normally incident on a U single-layer slab.

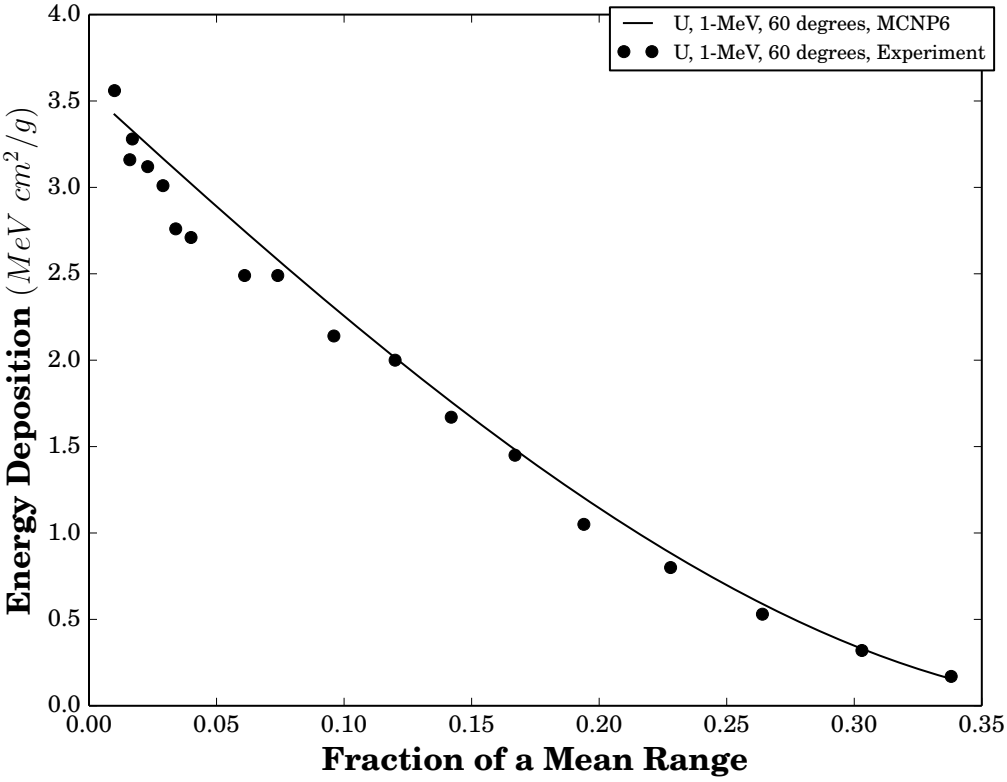

Figure 14: Energy deposition from 0.3- to 1-MeV electrons with 60 degrees off-normal incidence on a U single-layer slab.

B Relative Difference in Energy Deposition Profiles

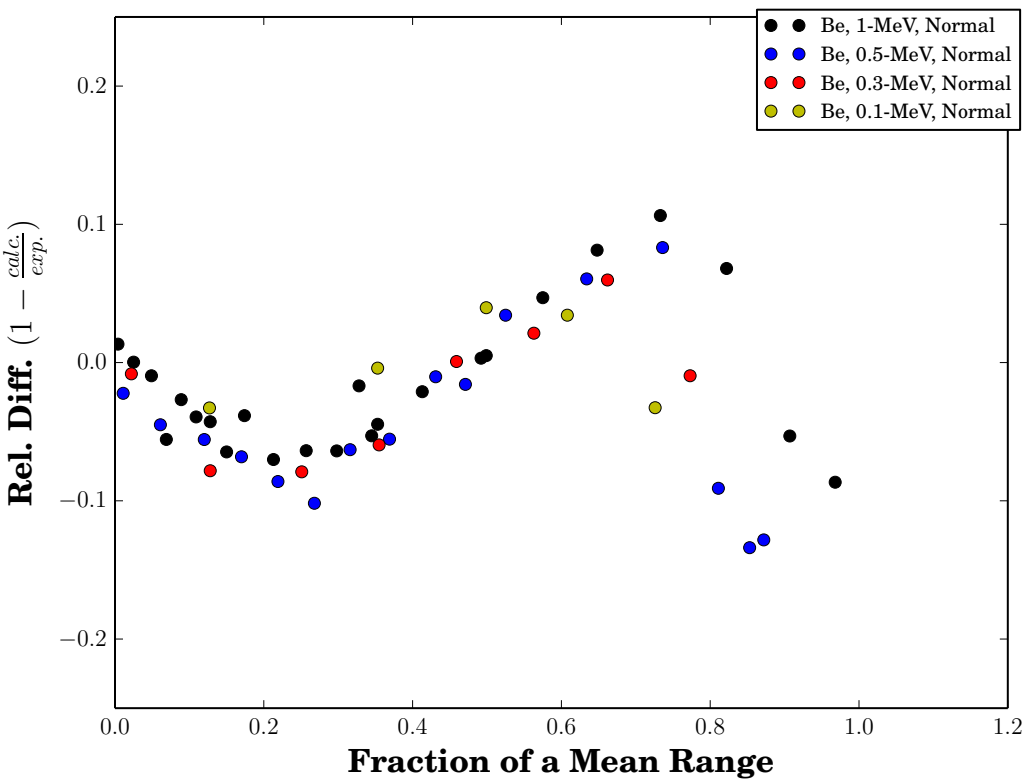

Figure 15: Relative difference in energy deposition from 0.1- to 1-MeV electrons normally incident on a Be single-layer slab.

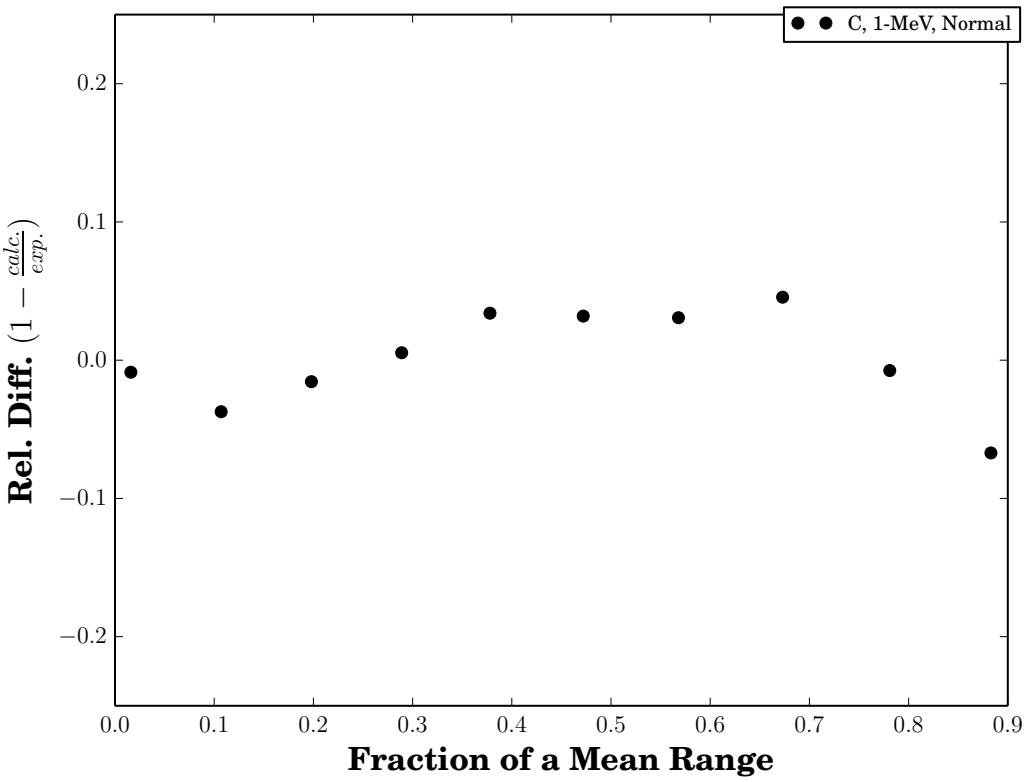

Figure 16: Relative difference in energy deposition from 1-MeV electrons normally incident on a C single-layer slab.

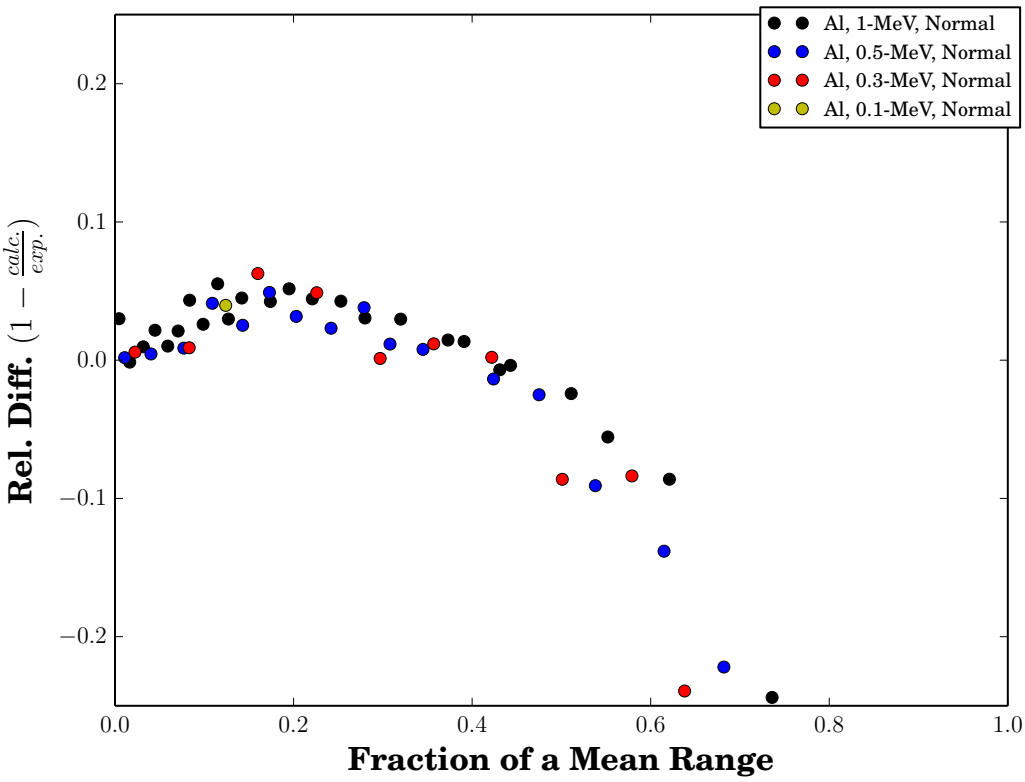

Figure 17: Relative difference in energy deposition from 0.1- to 1-MeV electrons normally incident on a Al single-layer slab.

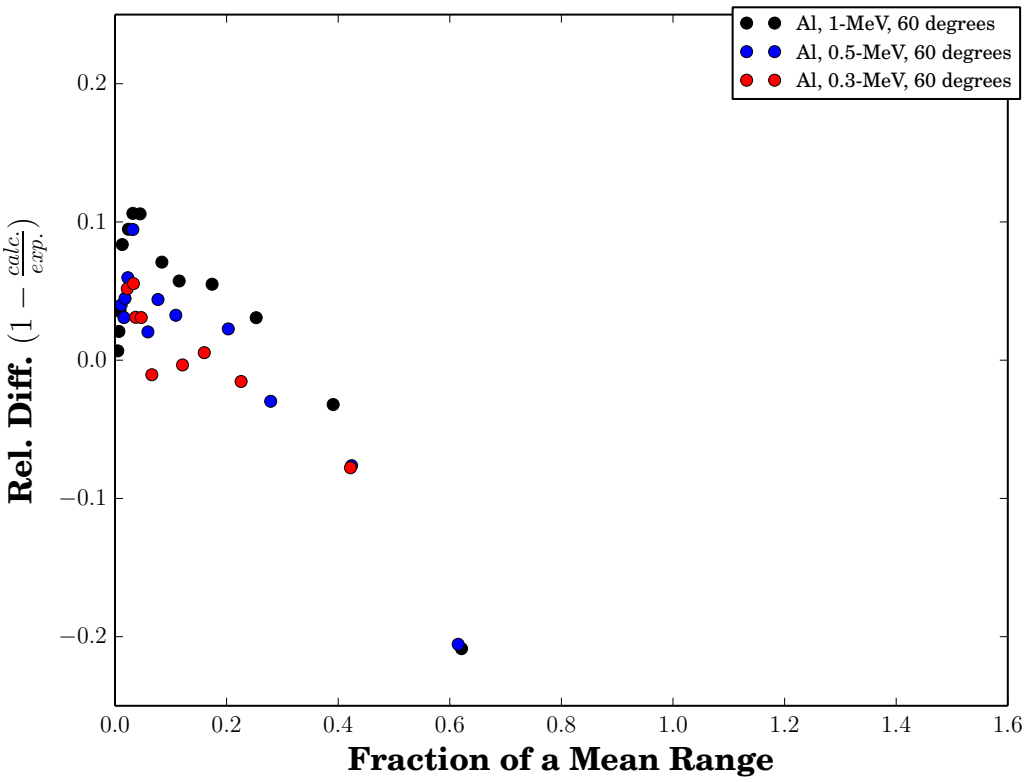

Figure 18: Relative difference in energy deposition from 0.3- to 1-MeV with electrons 60 degrees off-normal incidence on a Al single-layer slab.

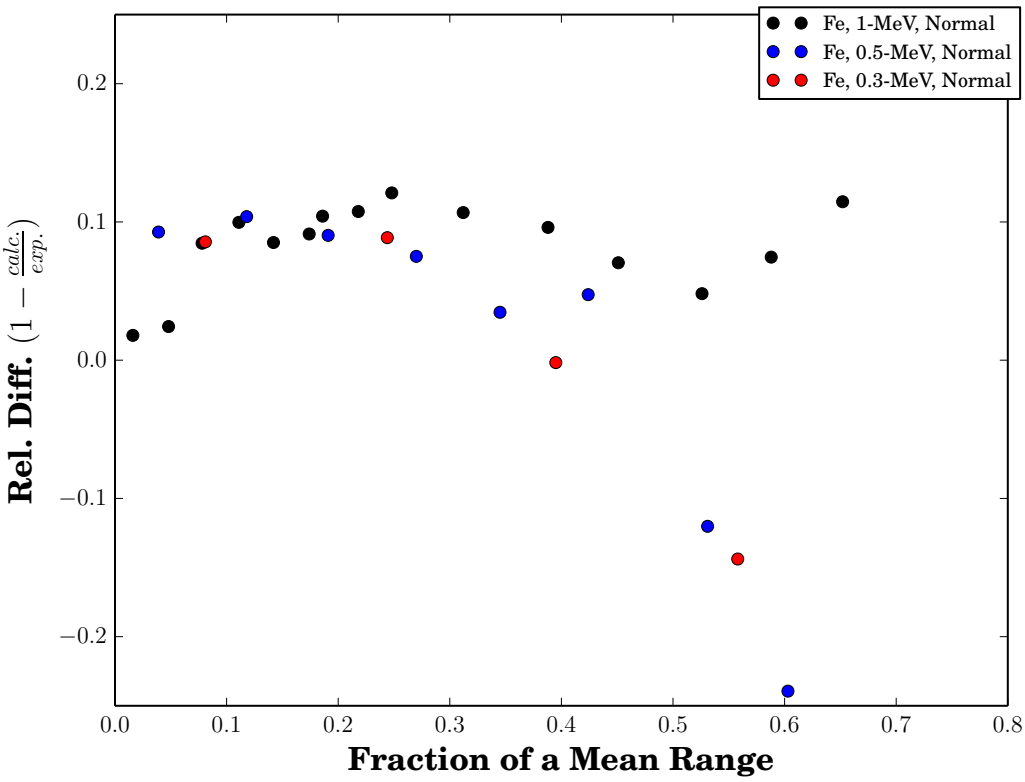

Figure 19: Relative difference in energy deposition from 0.3- to 1-MeV electrons normally incident on a Fe single-layer slab.

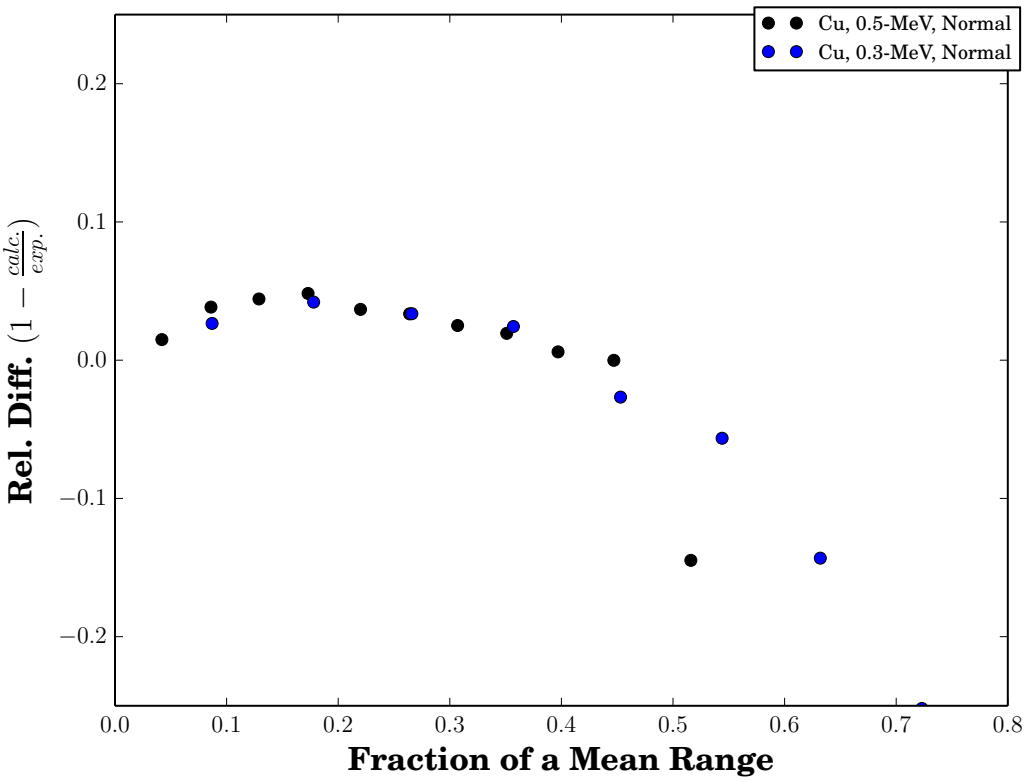

Figure 20: Relative difference in energy deposition from 0.3- to 0.5-MeV electrons normally incident on a Cu single-layer slab.

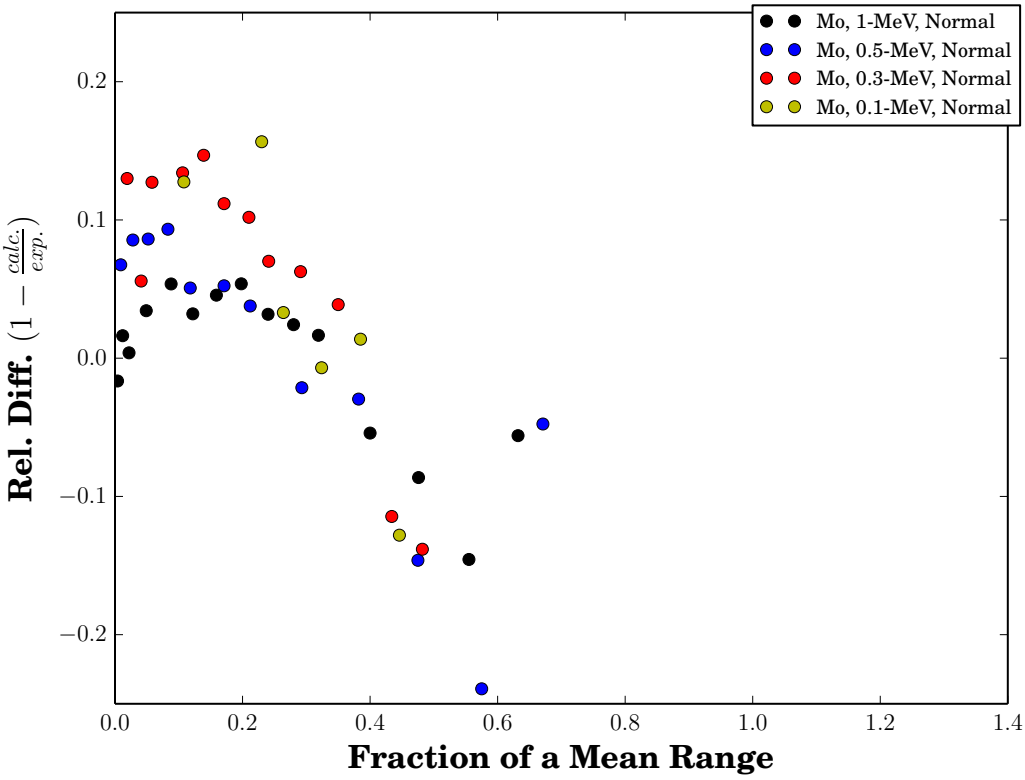

Figure 21: Relative difference in energy deposition from 0.1- to 1-MeV electrons normally incident on a Mo single-layer slab.

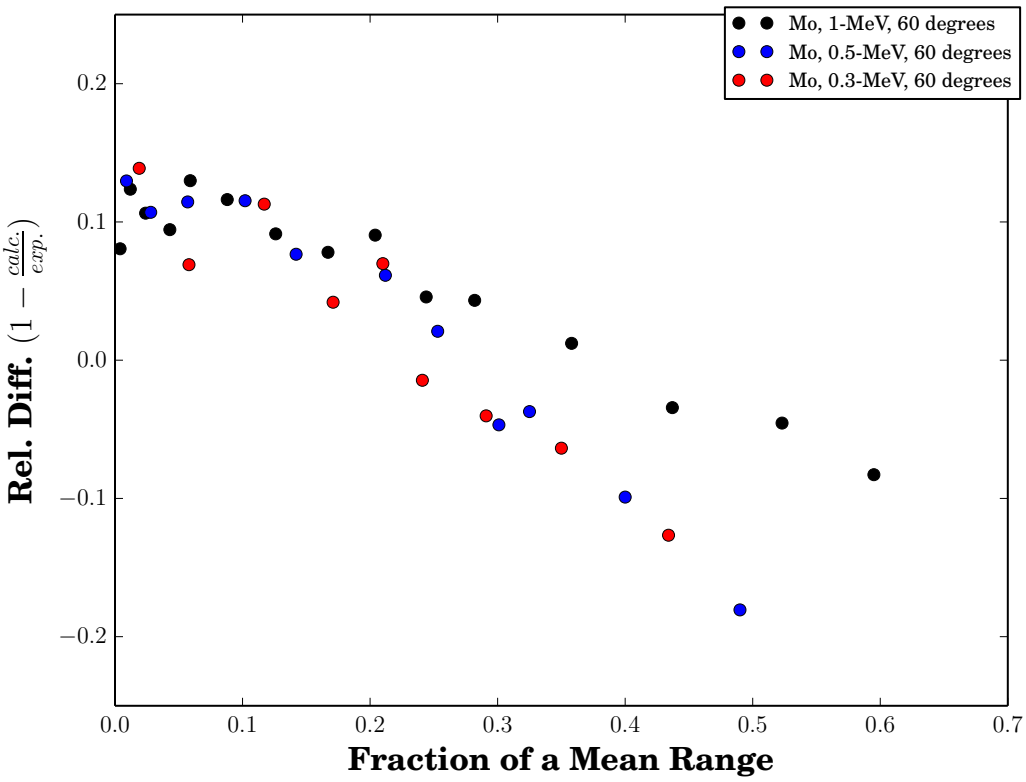

Figure 22: Relative difference in energy deposition from 0.3- to 1-MeV electrons with 60 degrees off-normal incidence on a Mo single-layer slab.

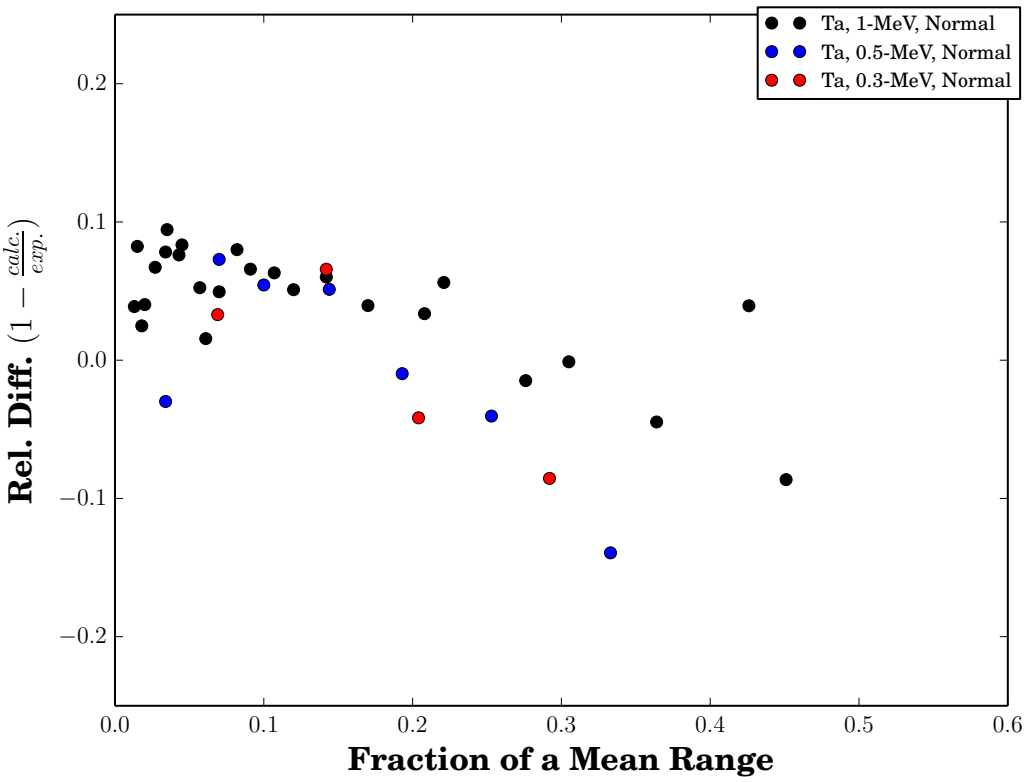

Figure 23: Relative difference in energy deposition from 0.3- to 1-MeV electrons normally incident on a Ta single-layer slab.

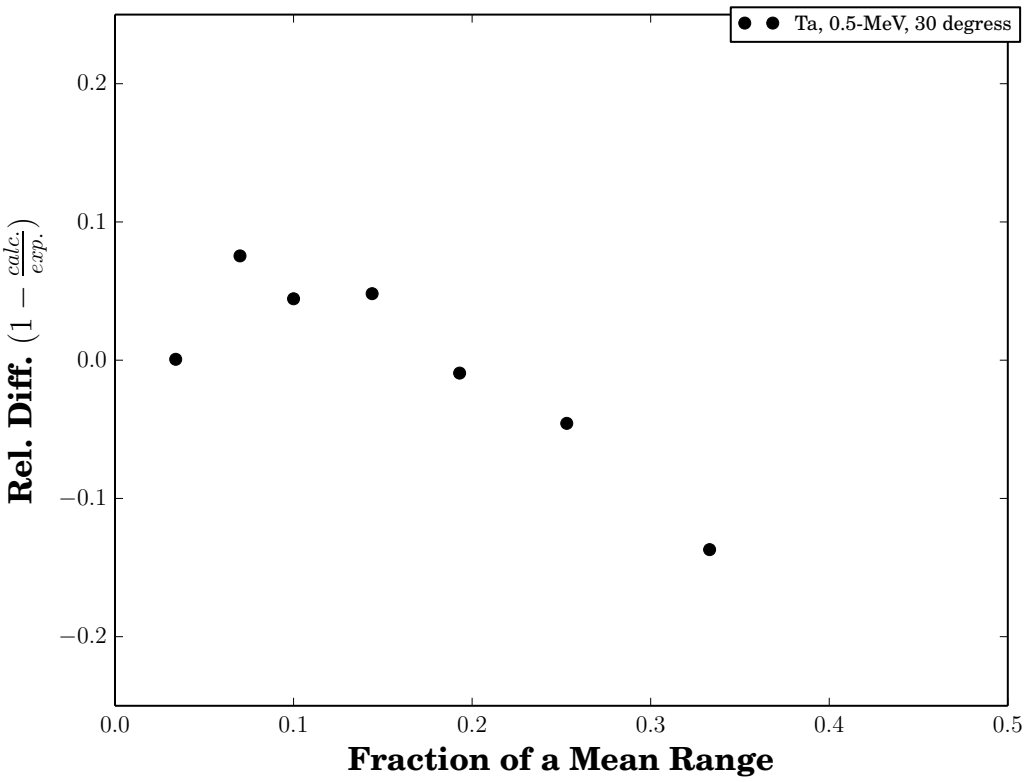

Figure 24: Relative difference in energy deposition from 0.5-MeV electrons with 30 degrees off-normal incidence on a Ta single-layer slab.

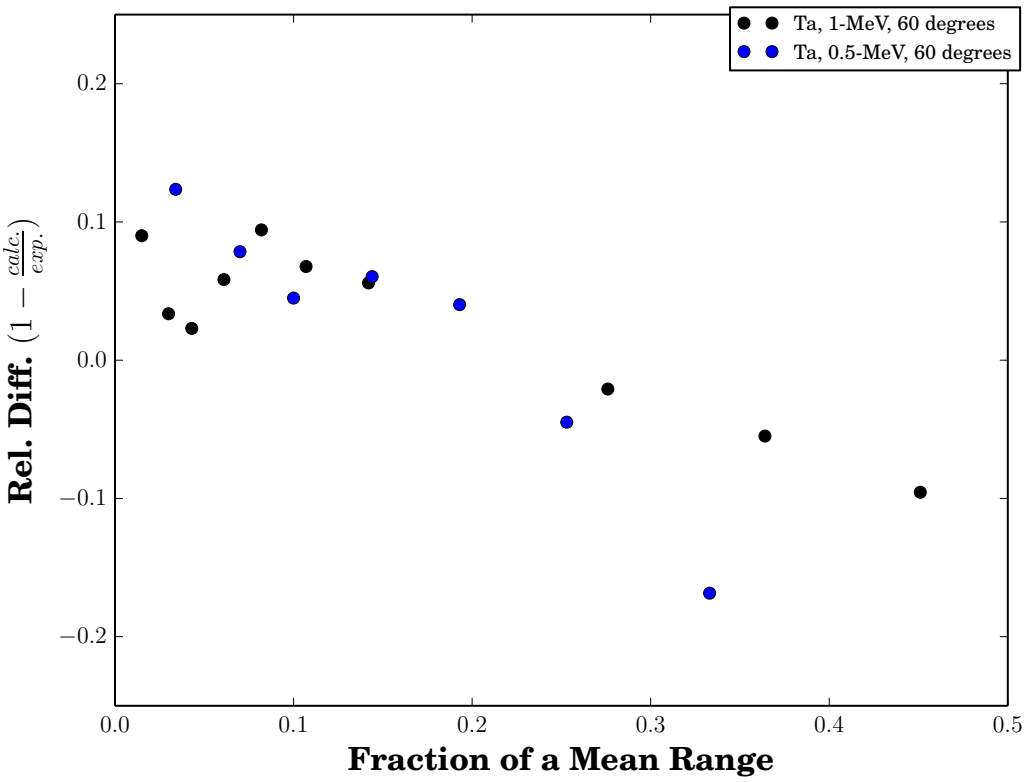

Figure 25: Relative difference in energy deposition from 0.5- to 1-MeV electrons with 60 degrees off-normal incidence on a Ta single-layer slab.

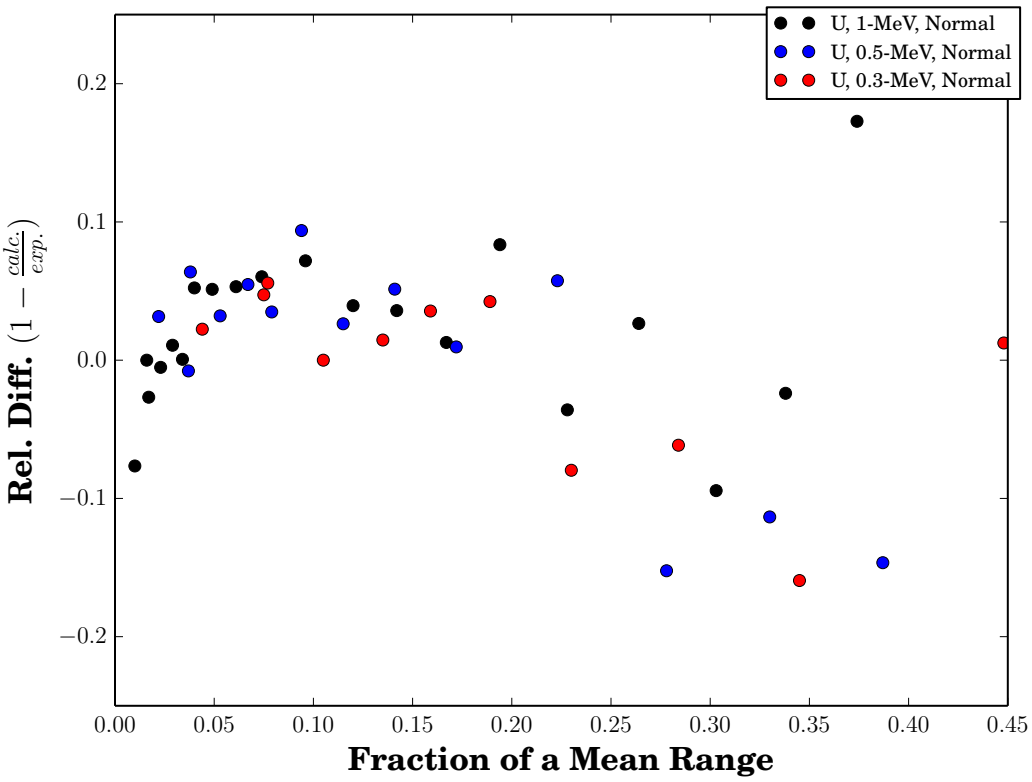

Figure 26: Relative difference in energy deposition from 0.3- to 1-MeV electrons normally incident on a U single-layer slab.

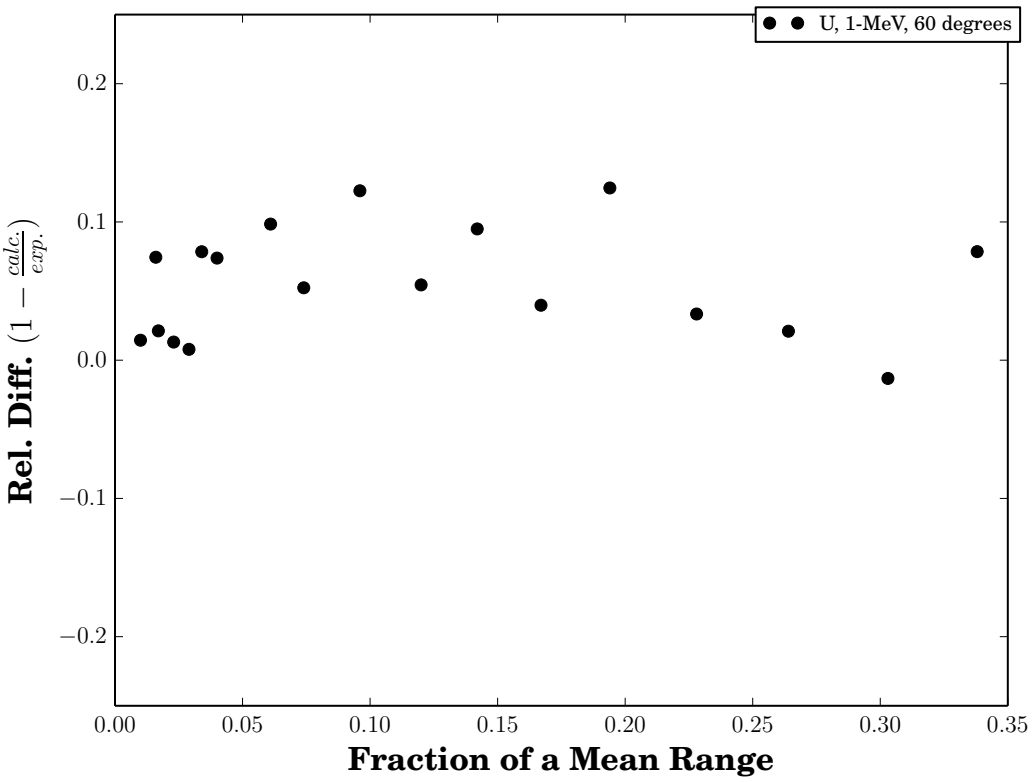

Figure 27: Relative difference in energy deposition from 1-MeV electrons with 60 degrees off-normal incidence on a U single-layer slab.